DEPLOYED PAYLOAD ANALYSIS FOR A SINGLE STAGE TO ORBIT SPACEPLANE

Federico Toso*, **Christie Alisa Maddock**†
Centre for Future Air Space Transportation Technologies
University of Strathclyde, Scotland, United Kingdom

The growth of the small satellite market requires an affordable and flexible launcher to satisfy the demand for insertion to a varied range of specific orbits. This paper presents the application and results of a tool created for the preliminary analysis of a reusable lifting body vehicle to address the demand of small to medium sized payloads. Trajectory optimisation is performed on the ascent mission of the launcher from a nominal cruise altitude to the release of the payload into different orbits with different mission and vehicle objectives and constraints. Two vehicle configurations are studied and applied to test cases of insertion to 200 km circular orbits at different inclinations. Further analysis on the performances obtained at different altitudes is conducted to study the effect on maximum payload mass. The advantages and limitations of the single stage to orbit approach are discussed and ways to overcome the latter are further analysed with the introduction of a small upper stage or tug. This additional engine can perform small manoeuvres to correct the flight path for orbital insertion, which expands the type of orbits that can be reached, and is integrated in the optimisation routine. The overall performance of the different launch systems are optimised for each mission, and compared against each other looking at the total payload mass and required mass fraction to reach different orbits.

I INTRODUCTION

One of the possible options to launch payloads into space has always been the single stage to orbit vehicle (SSTO). While there are many theoretical advantages, this type of vehicle has never been flown because of either technological obstacles or design complexity. The progress of material sciences, new manufacturing processes and the growth in computational performances of the new century are making the case of a commercial SSTO a viable one.

Conventional expendable rockets are limited on the mass fraction delivered to orbit by the rocket equation. Different options exist to increase the payload mass fraction, the most common is to introduce staging which can improve the overall mass fraction by splitting the ΔV gained in each stage.

A second option is one exploited by SSTO vehicles of increasing the effective exhaust velocity. Given the equation $v_e = I_{sp} g_0$ there can be up to a tenfold increase in efficiency[1] due to the fact that air-breathing engines do not have to carry the oxidizer onboard and thus have higher specific impulse. In addition, a lifting body can offset aerodynamic drag and gravitational losses using the lift generated by the wings. These losses may add up to 15% of the ΔV required to achieve orbit.

Improvements in propulsion technology, and demonstrations from companies like Reaction Engines with their SABRE pre-cooler proved that many of the integral components work both in theory and in practice; moving closer towards the realisation of high supersonic air-breathing engines. Moreover, while rockets are close to their ideal maximum efficiency and have improved relatively little in the last decades, supersonic and hypersonic air-breathing engines studies are still in their infancy and have plenty of room to improve.[2] Other advantages of the SSTO vehicles are derived from the horizontal take off and landing configuration that allows integration of the payload on the ground without tilting the vehicle, re-usability, abort capabilities designed to save both the launcher and the payload, reduced complexity due to absence of staging or air launch, and the promise of operations similar to commercial airliners with quick turnaround between missions.

This paper examines the trade-off between maximising the deployed payload mass and the operational orbits that can be reached from a given spaceport using a SSTO spaceplane vehicle. For each mission, the performance and trajectory of the launch vehicle is optimised in order to understand the sensitivity of the choice of orbit on the maximum payload mass and vehicle design.

*PhD student, federico.toso@strath.ac.uk
†Lecturer, christie.maddock@strath.ac.uk

The design methodology starts from this assumption in order to size the launcher: considering a variable margin for dry vehicle and payload, the propulsion, aerodynamic surfaces and initial mass are optimised with the objective of minimising the propellant needed for the mission. The mission is a full simulation of the trajectory, from the start of the ascent at the end of the cruise phase to the payload release in the desired orbit. The spaceport taken into consideration is Glasgow Prestwick, the choice is done to demonstrate the flexibility of this platform even for applications in high latitude locations that are less penalized for polar or sun-synchronous orbits but have a disadvantage for low inclination and equatorial orbits. Once the vehicle is sized for a LEO mission, the penalty of reaching other inclinations and altitudes is evaluated, discussing the reduction in payload capability. The reference missions analysed are for the launch of small satellites up to 1000 kg into a 200 km altitude Earth orbit, with two different inclinations taken into consideration. The mission is analysed starting after take-off and initial climb up to the release of the payload in the target operational orbit.

The optimisation is done using a highly modular code that can easily trade computational speed for model fidelity in each of the system models used.[3,4] The trajectory can be subject to multiple constraints that are easily modifiable for each mission such as no fly zones, maximum acceleration due to structural limitations, thermal flux and thermal load threshold as a consequence of the specific thermal protection system considered.

II SYSTEM MODELS

The mathematical models used in the mission optimisations are presented in the following section. The system models were developed for a preliminary analysis to work within a multidisciplinary design optimisation, and can be grouped into vehicle system models, including aerothermodynamics and propulsion, and operational and environment models for the Earth and atmosphere, and flight dynamics and control.

All the mathematical models used in this work are applied within a modular software environment, allowing a variable complexity with multiple levels of fidelity to satisfy the requirements during different phases of the mission, and to reduce the computation run time of the mission analysis.

II.I Vehicle configuration

The SSTO vehicle configuration was modelled based on a scaled down version of the Skylon D1 vehicle design using publicly available data and analyses. The Skylon D1 vehicle is a reusable SSTO designed by Reaction Engines to have the advantage of airline operations with easy payload integration thanks to horizontal take off and landing procedures and the advantage of using a highly efficient air breathing engine in the atmospheric phase of the ascent to increase the mass fraction brought to orbit. The SABRE engine is rated to generate $T = 2$ MN of thrust per nacelle, with two powerplants installed. The design gross take off weight is $m_{GTOW} = 325$ metric tons in the D1 configuration, 85% of which is the sum of fuels and payload, with the latter being $m_{Payload} = 15$ ton for an equatorial launch to a circular orbit of 300km with inclination $i = 0$. From a launch site positioned at a higher latitude $\lambda = 55$ deg, the mass in orbit decreases to $m_{Payload} = 13$ ton in a low inclination circular orbit of 200 km of altitude.

II.II Aerothermal

The aerodynamic forces are computed using the lift and drag coefficients for a conceptual hypersonic test vehicle Lazarus,[5] which focused on the development of aerodynamic laws for the purpose of scaling the performances of a SSTO vehicle in MDO. The validity of the value and method are dependent on the vehicle design. In the case here, the two vehicle configurations are similar enough to allow the values to provide a first approximation of the aerodynamic performances of a spaceplane with a maximum aerodynamic efficiency of 3. Using the standard equations for lift and drag forces, the coefficients are multiplied for the dynamic pressure $q = \frac{1}{2}\rho V^2$ of the fluid and the surface area S_{ref} of the wings, which is one of the design parameters involved in this study.

The thermodynamic model is responsible for the limitation of the trajectory upon atmospheric re-entry. The Sutton Graves equation[6] is a simplified method that conservatively assumes a fully catalytic surface to estimate the convective heating received by the wall. In the case of LEO re-entry of a lifting body, the contribution of the convective heating is many orders of magnitude higher than the radiative one that is therefore neglected.

$$q_{conv} = k \left(\frac{\rho}{R_n} \right)^{1/2} V^3 \qquad [1]$$

where $k = 1.7415 \times 10^{-4}$ for Earth's atmosphere.

With the increase in surface temperature, the body will start radiating heat following the Boltzmann law,

$$q_{rerad} = \epsilon\sigma \left(T^4 - T_\infty^4\right) \quad [2]$$

The emissivity $\epsilon = 0.8$ is set for a non ablative ceramic thermal protection and $\sigma = 5.67 \times 10^{-8}$ W/m^2/K^4 is the Stefan-Boltzmann constant. Neglecting the material response due to the lack of the ablation and charring processes, and with the reasonable assumption that the TPS is a particularly good insulator, the heat flux balance is assumed to be $q_{conv} = q_{rerad}$. From this relation, the wall temperature T_W can be determined.

$$T_W = \left(T_\infty^4 + \frac{q_{conv}}{\epsilon\sigma}\right)^{1/4} \quad [3]$$

While this effect is not affecting the ascent trajectories, analysis that focus on the re-entry phase or long duration hypersonic flight in the atmosphere are constrained to satisfy the limits of the chosen thermal protection system.

II.III Propulsion

Two propulsive modes are taken into consideration: air-breathing and rocket mode. The engine models have been created to fit publicly available SABRE datapoints.[7] The rationale that led to the selection of this particular engine are the same one that made Skylon the configuration of choice for this analysis. According to the Skylon User Manual, Rev 2.1, each of the nacelles in the air breathing mode is rated for a gross thrust from 0.8 to 2 MN, functioning from a standing start to Mach 5.5, with a specific impulse varying between 4000 and 9000 seconds. The rocket mode is less efficient, with a 450 s specific impulse, generating 2 MN of thrust. While the manual reports that this latter propulsive mode works from Mach 5.2 onward, it is most likely a consequence of the ascent profile of the Skylon vehicle, since the rocket engine would produce thrust independently of the flight speed.

Based on the available data, an approximate propulsive law is derived. The air-breathing mode of the engine model is set to reach peak efficiency at Mach 3.5 and 100% throttle and the decrease in atmospheric density negatively impacts the performances of the engine. This effect is achieved by lowering the specific impulse when the flight conditions change. The rocket engine does not have Mach dependence but has lower thrust at the higher pressure conditions found at low altitudes due to the nozzle expansion losses.

The last analysis presented introduces an upper stage with a small rocket powered orbital manoeuvring system for orbit insertion and correction. This engine model is set to generate a maximum force of $T = 4.9$ kN to avoid the possibility of having a thrust to weight ratio above one. The specific impulse $I_{sp} = 250$ s is a conservative assumption and a typical value for storable propellants which are not high efficiency engines but a common solution for payload integrated propulsion systems or upper stages that require multiple restarts. The nozzle exit area is assumed to have a diameter $d_e = 1$ m.

II.IV Environment

The WGS84 geodetic system is used considering the oblateness of the Earth spheroid for the determination of the radial distance of the Earth surface r_E. The gravitation model is based on spherical harmonics accounting for the J_2, J_3 and J_4 terms based on the radial distances to the Earth surface r_E and to the vehicle r, and the latitude λ. The gravitational acceleration is calculated for the radial and transversal components, $\mathbf{g} = g_r\hat{\mathbf{i}}_\mathbf{r} + g_t\hat{\mathbf{i}}_\mathbf{t}$.[8] The angular rotation of the Earth is assumed constant at $\omega_E = 7.292115 \times 10^{-5}$ rad/s.

The atmosphere is modelled using the globally averaged International Standard Atmosphere. For each value of flight altitude, there is a corresponding output of pressure and temperature used to compute density and sound speed. The ISA is a valid model till $h = 84852$ m, above which the altitude pressure and density are set to zero, while temperature is fixed to $T = 186.87$ K to limit the speed of sound to a constant value.

II.V Flight dynamics and control

The vehicle is modelled as a point mass in an Earth Centered Earth Fixed (ECEF) reference frame with 3 degrees of freedom for all the phases of the mission. The dynamics for the transatmospheric flight are the same for ascent or descent. Within this model, the spaceplane is considered as a point with a time-varying mass centred on the Centre-of-Mass of the vehicle. The set of equations of motion are calculated within a geocentric rotating reference frame using spherical coordinates, denoted by $\mathcal{F}$.

The state vector for the position and velocity is $\mathbf{x} = [h,\, \lambda,\, \theta,\, v,\, \gamma,\, \chi]$ where h is the altitude (the radial distance is $r = h + R_\text{E}$), (λ, θ) are the geodetic latitude and longitude, v is the magnitude of the relative velocity vector directed by the flight path angle

γ and the flight heading angle χ. The equations of motion are given by,[8]

$$\dot{h} = \dot{r} = v \sin\gamma \tag{4a}$$

$$\dot{\lambda} = \frac{v \cos\gamma \sin\chi}{r} \tag{4b}$$

$$\dot{\theta} = \frac{v \cos\gamma \cos\chi}{r \cos\lambda} \tag{4c}$$

$$\dot{v} = \frac{F_T \cos(\alpha+\varepsilon) - D}{m} - g \sin\gamma + \omega_e^2 r \cos\lambda \left(\sin\gamma \cos\lambda - \cos\gamma \sin\chi \sin\lambda\right) \tag{4d}$$

$$\dot{\gamma} = \frac{F_T \sin(\alpha+\varepsilon) + L}{mv} \cos\mu - \left(\frac{g}{v} - \frac{v}{r}\right) \cos\gamma + 2\omega_{\mathrm{E}} \cos\chi \cos\lambda + \omega_{\mathrm{E}}^2 \left(\frac{r}{v}\right) \cos\lambda \left(\sin\chi \sin\gamma \sin\lambda + \cos\gamma \cos\lambda\right) \tag{4e}$$

$$\dot{\chi} = \frac{L}{mv\cos\gamma} \sin\mu - \left(\frac{v}{r}\right) \cos\gamma \cos\chi \tan\lambda + 2\omega_{\mathrm{E}} \left(\sin\chi \cos\lambda \tan\gamma - \sin\lambda\right) - \omega_{\mathrm{E}}^2 \left(\frac{r}{v\cos\gamma}\right) \cos\lambda \sin\gamma \cos\chi \tag{4f, 4g}$$

where α is the angle of attack, μ is the bank angle, m is the mass of the vehicle, ε is the pitch offset angle between the direction of thrust F_T and the longitudinal plane of the vehicle, g is the gravitational acceleration, and L and D are the aerodynamic lift and drag forces, respectively. With the exception of ε, all the terms are time-varying. F_T is the magnitude of the thrust given by the engine.

Looking at a standard aircraft body-relative reference frame $\mathcal{B}$, $+x^{\mathcal{B}}$ is towards the nose along the longitudinal axis of the spaceplane, $+y^{\mathcal{B}}$ is outwards along the wing, and $+z^{\mathcal{B}}$ points downwards towards the Earth normal to the plane of symmetry given by $x^{\mathcal{B}}$-$y^{\mathcal{B}}$. The flight path angle is the angle between the local horizon (defined by as the plane tangent to the radial vector) and the velocity vector, while the flight heading angle is the angle between North (or the $x^{\mathcal{F}}$-axis) and the horizontal component of the velocity vector.

The orbital parameters necessary to compute the constraints relative to the final operational orbits are computed with a conversion of the local east-north-up coordinates to the ECEF spheroid-centric Cartesian. The rotation of the earth is added to obtain the Earth Centered Inertial expression required to calculate the required orbital elements of semimajor axis a, eccentricity e and inclination i. With this additional information is possible to introduce the constraints needed to obtain circular and sun synchronous orbits.

III OPTIMISATION APPROACH

A multidisciplinary optimisation was used to evaluate the performance of the vehicles. The trajectory is divided into multiple phases, each with specific optimisation settings and models to best represent the system and environment. This approach can be used to handle mathematical singularities such as the aerodynamic coefficient at transonic speeds by having a subsonic phase followed a supersonic one with enforced matching constraints on the state variables, simulate staging with instantaneous mass changes or to switch propulsion models such the one here from the air-breathing to rocket mode. Every phase is set up to have specific mathematical models for the environmental variables, the aerodynamic and propulsive forces, thermal constraint evaluations, dynamic equations, number of multi-shooting elements, control nodes in each element, minimum and maximum bounds for states and controls and time of flight.

III.I Optimal control

The optimal control problem is formulated with a direct transcription, multiple shooting method in which every phase is divided into n_m segments with n_c discrete control nodes. The time of flight of each segment is an optimisation variable, and is used to derive the time distribution of the control nodes based on a Tchebycheff distribution which biases the points towards the two extremes of the segments. Conditions are added to match the state and control variables between segments, dependant on the formulation of the phases. For example, to account for mass drops during staging, the matching condition for the vehicle mass is removed.

Each segment is numerically integrated using a 4th order Runge Kutta with a fixed time step. The value of the timestep is an input variable and can be set depending on the phase analysed, allowing larger time steps for phases such as a coasting arc.

The controls are determined using a piecewise cubic Hermite interpolation of the open loop control law.

III.II Local optimisation

The optimisation of the problem is performed using Matlab nonlinear constrained optimisation function `fmincon` using an interior point method. The cost function is the maximisation of the mass fraction delivered to orbit. Maximizing this value minimises the

propellant mass used for the ascent once either the final (dry) or the initial gross take-off masses are fixed.

Equality constraints are added to ensure that the relevant state and control variables are connected between elements of the trajectory (phases and shooting segments) and that the final orbit is reached based on matching the semi-major axis, eccentricity and inclination.

Inequality constraints are set to ensure the thermal limits of the TPS are satisfied, $T_W \leq 2000$ K, and that the axial and normal accelerations induced on the vehicle $a_{x,z} \leq 6g_0$. A constraint is set to ensure the final mass is higher than the dry mass of the vehicle, $m(t = t_f) \geq m_{dry}$.

III.III First guess

The first guess is selected by performing a multi-start global search. The number of sample points is increased linearly with the growth of the number of variables of the problem. The starting values are distributed on the search space using the latin hypercube sampling technique to better explore the search space. To efficiently sort through all the starting points, a large simulation timestep is used to reduce the computational run time. In addition, the optimisation tolerances on the constraints are relaxed and the maximum number of iterations reduced to achieve a fast selection of the first guesses.

Once the multiple starting points have been evaluated and the best local solution has been found, this solution is re-optimised using an iteratively reduced timestep until a minimum timestep is reached (based on the input criteria) with tightened (or un-relaxed) constraints. This incremental increase in complexity greatly reduces computational time required to generate a feasible first guess while adding some exploration capabilities to the optimisation process.

IV TEST CASE

The setting for the ascent optimisation of the SSTO are listed in Table 1. The unconstrained heading angle is an advantage of the lifting body vehicle that can initiate the ascent procedure from a level flight in the optimal direction. Starting latitude and longitude are set to be in a small area around the departure spaceport of Glasgow Prestwick.

IV.I Vehicle scaling

For the first analysis, used to size the vehicle, the mass at the start of the ascent phase is an optimisation parameter. Since the cost function of the optimisation is the minimisation of the fuel used for ascent, the dry mass of the vehicle has to be constrained. The dry weight to GTOW ratio of the Skylon vehicle is 15% and assuming this baseline value, a penalty coefficient of 4.44% per 100 metric tons was imposed. While it can be argued that the mass increase due the size reduction does not take into account fixed contribution of the avionics and other constant weights, there is a compensating effect due to the decrease of the thickness of the thermal protection system. While the weight scales with the third power of the linear measure, the surface scales with the square of the length, guaranteeing a lower ballistic coefficient. The sizing is performed aiming to deliver a 1 ton payload to a low inclination circular orbit of 200 km. The optimised value of starting mass found is $m_0 = 90035$ kg, not accounting for the fuel needed for ascent from the runaway to the starting simulation altitude.

A simple scaling of the masses would leave the vehicle with overestimated aerodynamic and propulsive forces. To eliminate the issue and further study the optimal configuration, a variable is introduced to scale the performance of the engine and the aerodynamic surfaces. The scaling factor is the same for the forces generated by the wings and by the engines. This avoids an excessive reduction of the wings whose contribution in the ascent phase is much smaller compared to that of engine. This protects the necessary wing area, giving a suitable L/D ratio assuming a glided descent phase.

The optimal configuration is found scaling to 96.11% of the forces generated by Skylon's wings and SABRE thrust. This configuration reaches LEO at 200 km with a final mass of $m_f = 24189$ kg including payload. The high values of the forces does not violate the 6g acceleration limit imposed along the trajectory (along both the axial and normal directions), a standard value of many payload launchers, and allows a substantial reduction of gravity losses with a fast ascent since most of the aerodynamic losses are in the early phases of low altitude flight.

The engine mode switch of the trajectory used for sizing was found to occur at 2340 m/s at an altitude of $h = 51.02$ km. The end of the air-breathing phase is intentionally left as an unconstrained optimisation parameter. Figures 3(f) and 3(h) for the 400 km circular orbit illustrate how the unusually high switching altitude is an artefact of the optimiser exploiting the engine model outside of the expected operational range. The function used to calculate the thrust in air-breathing mode can generate a small amount of

Table 1: Boundary conditions on state and control variables for the SSTO vehicle reaching a 200km orbit

Variable	**Initial conditions**	**Bounds per phase**	
		Phase 1 (air breathing)	Phase 2 (rocket)
Altitude, h	$h_0 = 12$ km	[1, 50] km	[20, 200] km
Latitude, λ	free	$[+52, +58]$ deg N	$[-90, +90]$ deg N
Longitude, θ	free	$[-8, -2]$ deg E	$[-180, +180]$ deg E
Relative velocity, v	$v_0 = 210$ m/s	$[150, 2500]$ m/s	$[1500, 7500]$
Flight path angle, γ	$\gamma_0 = 0$ deg	$[-60, +90]$ deg	$[-60, +90]$ deg
Flight heading angle χ	free	$[-180, +180]$ deg	$[-180, +180]$ deg
Vehicle mass, m	$m_0 = 90035$ kg	$[m_{dry}, m_{gtow}]$	$[m_{dry}, m_{gtow}]$
Angle of attack, α	–	$[-10, +30]$ deg	$[-10, +30]$ deg
Engine throttle, τ	–	$[0, 1]$	$[0, 1]$
Control elements, ne	–	2	2
Control nodes, nc	–	7	7
Time of flight, Δt	–	$[120, 600]$ s	$[120, 600]s$

force more efficiently than the rocket motor in a narrow region outside of the desired operating regime. After this point in the high supersonic regime, the engine is switched to the rocket operational mode till the end of the main ascent phase. Despite this, the quality of the solution is shown by the low inclination of the final orbit on the ground track in the latitude-longitude plane and from the coasting arc before the final circularisation burn to enter the orbit. With more accurate propulsion models, the algorithm can be a useful tool to aid the choice of the optimal switching point.

IV.II Payload analysis in different orbits

After sizing the vehicle and having fixed the parameters that influence the forces, the penalty to access different orbits is studied. Each of the analysed orbits is computed with a dedicated optimisation run to evaluate the mass margin available. The mass margins are studied relative to the different characteristic orbital energies computed with the formula $C_3 = v^2 - \mu_E/r$ where μ_E is the standard gravitational parameter of the Earth and r and v are the radial distance and velocity relative to the inertial frame of reference. Each value of C_3 energy identifies a group of orbits by combining the contribution of different orbital parameters and is an effective figure of merit in tradeoff studies.

From the obtained results in Fig. 1 we can see how sensitive the design margin of a 1 ton payload is, and how by slightly increasing the target orbit altitude or inclination, the available payload mass is quickly reduced to negative values. To mitigate this issue, one of the possibilities is to design a larger vehicle that can carry more fuel in order to access high inclination orbits such as the sun synchronous (SSO).

Using the same approach detailed in the previous section, a second vehicle is designed choosing a retrograde sun synchronous circular orbit with an altitude of 200 km as target for the same amount of payload. The result obtained is a SSTO vehicle with a initial mass $m_0 = 147650$ kg and a force fraction of 99%. As seen in Fig. 1, this new configuration is able to achieve a sun synchronous orbit, and deliver a payload greater than 1 ton to lower inclinations. The heavier 150 t vehicle shows the same drop-off trend in mass fraction with an increase in altitude as the 90 t vehicle.

IV.III Addition of an upper stage

A commonly used solution to extend the capabilities of the launcher to allow the payload to reach orbits that require more energy is staging. Breaking the mass fraction of the rocket equation in two parts allows a great gain in quantity of payload delivered above the SSTO design point. To demonstrate this effect, a small upper stage is introduced that can either be an expendable vehicle or part of the actual

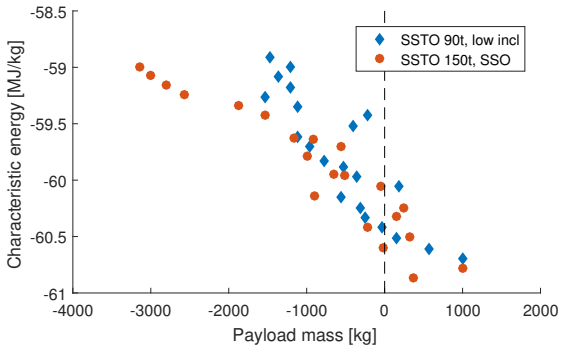

(a) Payload delivered by the SSTO to different orbits at the respective design inclination.

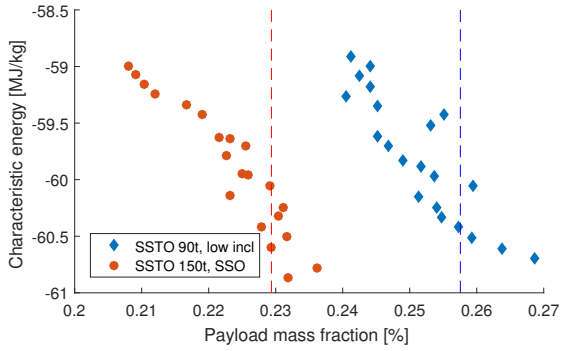

(b) Remaining mass fraction at orbit insertion.

Fig. 1: Results obtained for different target orbits between $h = 200$ km and $h = 400$ km by the two vehicle configurations, expressed as both residual payload and mass fraction. Dashed lines highlight the respective dry mass limits and fractions.

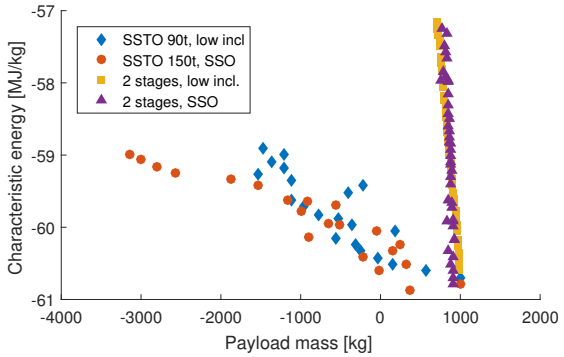

(a) Comparison of the vehicle configurations with and without upper stage for both sun synchronous and low inclination orbits from $h = 200$ km to $h = 600$ km.

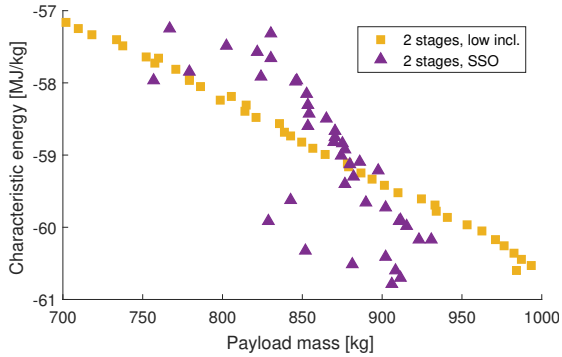

(b) Zoomed area of Fig. 2(a) highlighting the performances of the 2 staged approach for both SSO and low inclination orbits between $h = 200$ km and $h = 600$ km.

Fig. 2: Performances obtained by the SSTO vehicle and the approach with two stages, with a more detailed view of the latter.

payload that could also be used for end of life decommissioning.

The performance metric analysed, the final mass, includes the payload spacecraft, the propulsive system and any required subsystem needed for the operations after release from the reusable launcher stage. A coasting phase without thrust is introduced in the optimisation routine at the end of the ascent of the first vehicle that was designed for 1000 kg of payload in a $h = 200$ km low inclination circular orbit. This unpowered phase has only one control node to link the angle of attack and bank angle from upper stage release to the final circularisation phase. This last flight segment has the task of performing a burn on the apogee to raise the perigee of an elliptical orbit till the value of eccentricity is $e = 0$.

The analyses have been performed from $h = 200$ km to $h = 600$ km for both the low inclination and the sun synchronous orbit groups, while the computation for the SSTO cases simulations were halted at $h = 400$ km with a negative final payload mass. The optimal trajectory for the insertion in the $h = 400$ km low inclination orbit is shown in Fig. , where the coasting arc extends in the circularisation phase by throttling down the engine till the final moments of the ascent where the last burn is performed. The sudden drop in mass in Fig. 3(e) is due to the fact that the first stage mass is ignored after staging.

Table 2: Additional Boundary Conditions and Bounds on State and Control Variables for the introduction of the upper stage targeting a 200km orbit

Variable	**Bounds per phase**	
	Phase 3 (coasting)	Phase 4 (circularization)
Altitude, h	$[50, 600]$ km	$[100, 600]$ km
Latitude, λ	$[-90, +90]$ deg N	$[-90, +90]$ deg N
Longitude, θ	$[-180, +180]$ deg E	$[-180, +180]$ deg E
Relative velocity,v	$[5000, 8000]$ m/s	$[5000, 8000]$
Flight path angle, γ	$[-60, +90]$ deg	$[-60, +90]$ deg
Flight heading angle χ	$[-180, +180]$ deg	$[-180, +180]$ deg
Vehicle mass, m	$[100, 1000]$	$[100, 1000]$
Angle of attack, α	$[0, 0]$ deg	$[-30, +30]$ deg
Engine throttle, τ	$[0, 0]$	$[0, 1]$
Control elements, ne	1	1
Control nodes, nc	1	7
Time of flight, Δt	$[0, 1200]$ s	$[0, 600]s$

IV.IV Upper stage performance analysis

As can be seen in Fig 2(a), the introduction of the upper stage produces a drastic increase of the orbits that can be reached by the payload with a small sacrifice in final mass. This behaviour greatly offsets the penalty of altitude, allowing small payloads to reach high energy orbits. A magnification of the area of the new datapoints is shown in Fig. 2(b), highlighting how even for the high altitude $h = 600$ km orbits the final mass is still positive and $m_f \geq 700$ kg.

While the increase in payload due to the addition of an extra stage is obvious, the particularly interesting result is the fact that the trajectories are numerically evaluated case by case, and most of the solutions found are lined up on a front that can be considered a good performance metric for the robustness of the optimisation routine, especially in the low inclination orbit group. An additional confirmation can be deducted by the fact that the solution for the 200 km low inclination case are extremely close to the 1000 kg value found without the upper stage even though no information were used from the SSTO case to generate the new data.

V CONCLUSION

A modular MDO approach was used to evaluate the performance of a SSTO vehicle examining the payload mass that can be delivered against different orbits, using the vehicle mass fraction against the characteristic energy of the orbit.

A reference vehicle design was obtained for a reference orbit. This vehicle was then used to analyse the performance at higher altitude and different inclination orbits, extrapolating a set of solutions that analysed on the payload-energy graph show the performances and limitations of the approach. The sharp decrease in payload due to the final altitude increase is mitigated by the introduction of an additional stage that drastically reduces the effect.

From these preliminary results, it is shown how designing a vehicle for a specific orbit limits the possibilities to expand the range of operations outside of the predetermined bounds and, if some effects are not taken into account, a vehicle may be unable to meet the expectations of a varied set of customers.

REFERENCES

[1] Segal, C., *The scramjet engine: processes and characteristics*, Vol. 25, Cambridge University Press, 2009.

[2] Varvill, R. and Bond, A., "A comparison of propulsion concepts for SSTO reusable launchers," *Journal of the British Interplanetary Society*, Vol. 56, No. 3/4, 2003, pp. 108–117.

[3] Pescetelli, F., Minisci, E., Maddock, C., Taylor, I., and Brown, R., "Ascent Trajectory Optimisation for a Single-Stage-to-Orbit Vehicle with Hybrid Propulsion," *AIAA/3AF International Space Planes and Hypersonic Systems and Technologies Conference*, 2012.

[4] Toso, F., Maddock, C., and Minisci, E., "Optimisation of Ascent Trajectories for Lifting Body Space Access Vehicles," *Space transportation solutions and innovations symposium, International Astronautical Congress*, 2015.

[5] Young, D. A., Kokan, T., Clark, I., Tanner, C., and Wilhite, A., "Lazarus: A SSTO Hypersonic Vehicle Concept Utilizing RBCC and HEDM Propulsion Technologies," *International Space Planes and Hypersonic Systems and Technologies Conference*, AIAA, 2006.

[6] Sutton, K. and Graves Jr, R. A., "A general stagnation-point convective heating equation for arbitrary gas mixtures," 1971.

[7] Hempsell, M., Longstaff, R., and Bond, A., "SKYLON Users Manual," *Reaction Engines Limited*, Vol. 1, 2010.

[8] Tewari, A., *Atmospheric and space flight dynamics*, Springer, 2007.

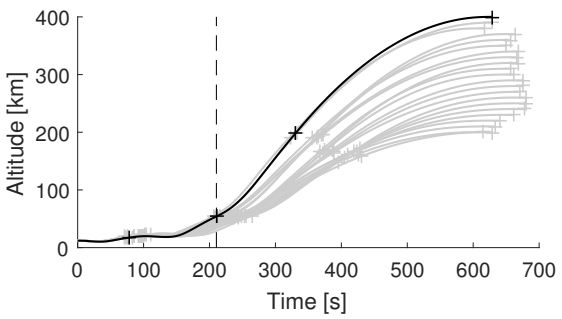

(a) Altitude time history

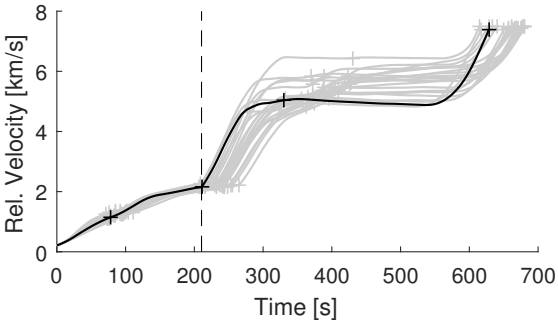

(b) Velocity time history

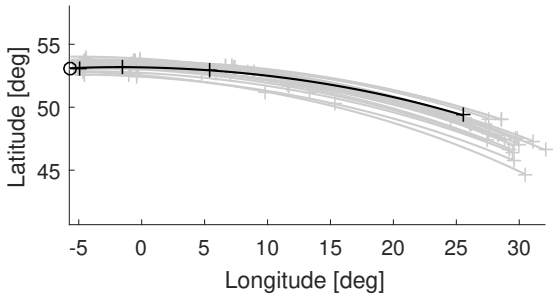

(c) Ground Track on the latitude-longitude plane, circle marks the starting point

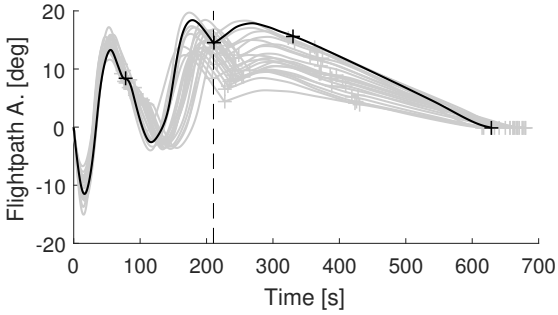

(d) Flight path angle time history

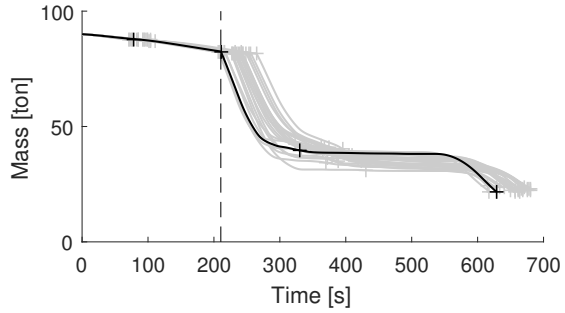

(e) Mass time history

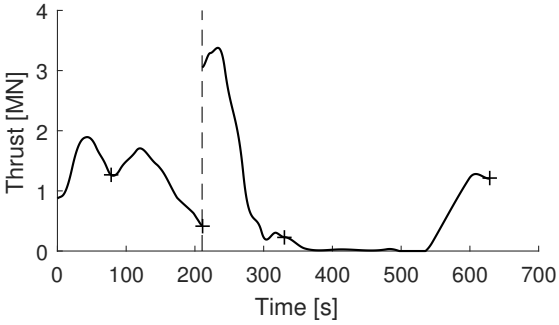

(f) Thrust time history

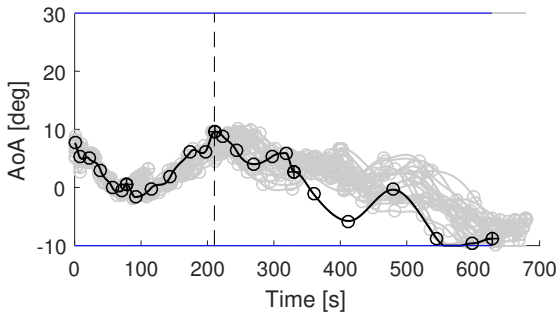

(g) Angle of attack time history

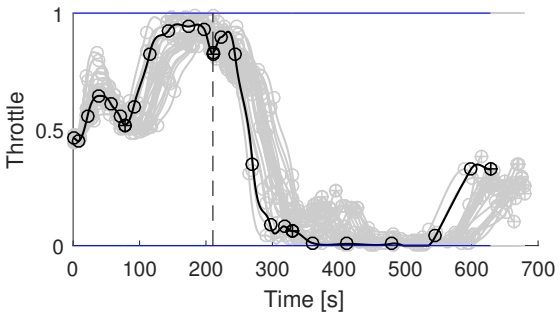

(h) Throttle time history

Fig. 3: Time history of the states and controls for SSTO trajectories with different low inclination target orbits, highlighted the 400km one. Engine model changes on the dashed line.

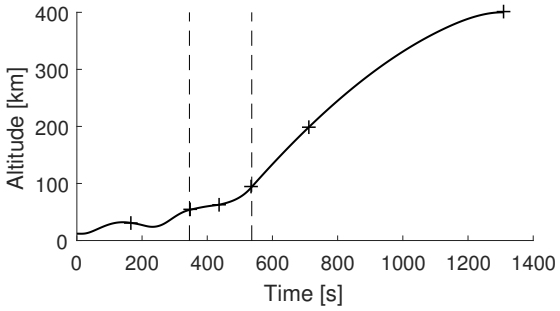

(a) Altitude time history

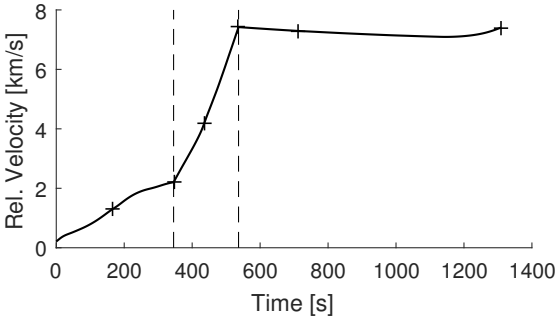

(b) Velocity time history

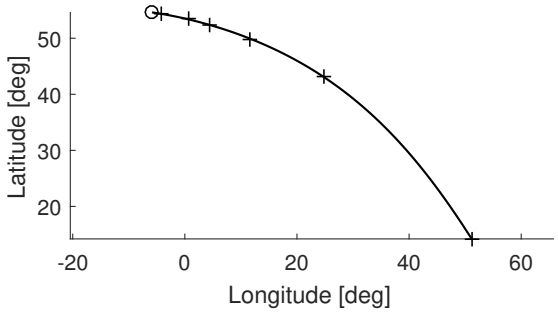

(c) Ground Track on the latitude-longitude plane, circle marks the starting point

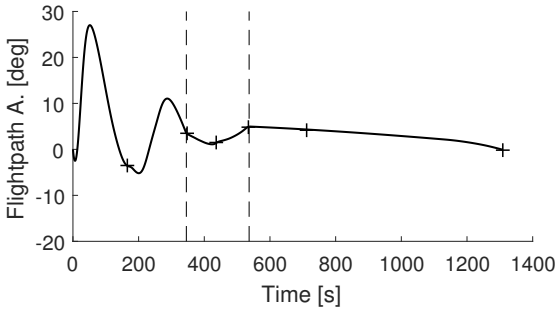

(d) Flight path angle time history

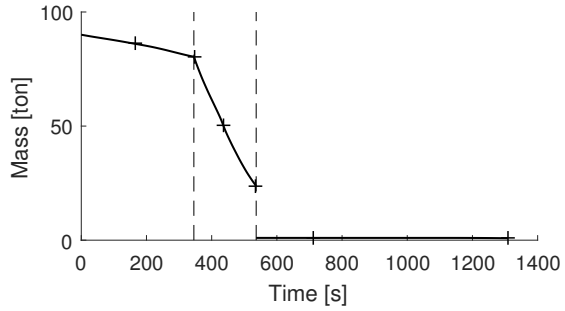

(e) Mass time history

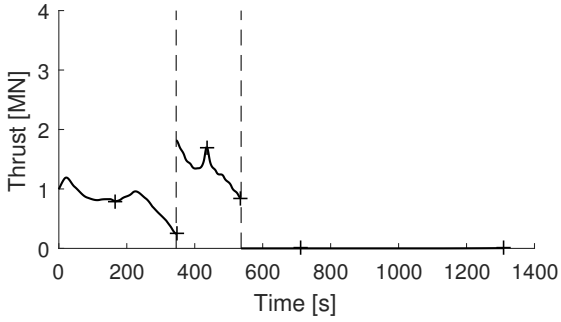

(f) Thrust time history

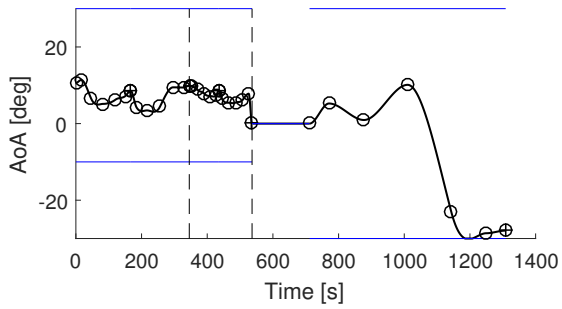

(g) Angle of attack time history

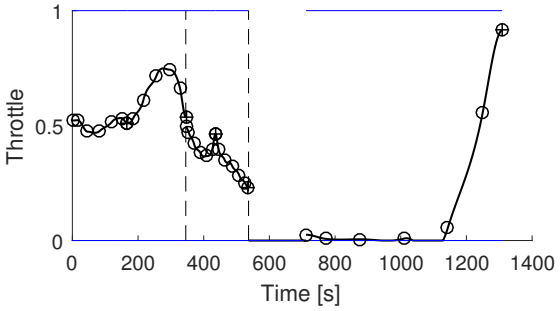

(h) Throttle time history

Fig. 4: Time history of the states and controls for SSTO+TUG trajectories with different low inclination target orbits, highlighted the 400km one. Engine model changes and staging on the dashed lines.